nature climate change

ARTICLES

https://doi.org/10.1038/s41558-018-0084-2

Climate-driven range shifts of the king penguin in a fragmented ecosystem

Robin Cristofari[1,2,3,4], Xiaoming Liu[5], Francesco Bonadonna[6], Yves Cherel[7], Pierre Pistorius[8], Yvon Le Maho[1,2,3], Virginie Raybaud[9,10], Nils Christian Stenseth[4], Céline Le Bohec[1,2,3,13,14*] and Emiliano Trucchi[4,11,12,13,14*]

Range shift is the primary short-term species response to rapid climate change, but it is often hampered by natural or anthropogenic habitat fragmentation. Different critical areas of a species' niche may be exposed to heterogeneous environmental changes and modelling species response under such complex spatial and ecological scenarios presents well-known challenges. Here, we use a biophysical ecological niche model validated through population genomics and palaeodemography to reconstruct past range shifts and identify future vulnerable areas and potential refugia of the king penguin in the Southern Ocean. Integrating genomic and demographic data at the whole-species level with specific biophysical constraints, we present a refined framework for predicting the effect of climate change on species relying on spatially and ecologically distinct areas to complete their life cycle (for example, migratory animals, marine pelagic organisms and central-place foragers) and, in general, on species living in fragmented ecosystems.

Anthropogenic global environmental change is known to have important consequences for biological communities[1], yet the nature and extent of species' responses are still poorly understood[2]. Species' responses to climate change are contingent on intrinsic sensitivity and plasticity[3] as well as on the spatial complexity of their habitats[4]. In particular, the synergy between climate change and habitat fragmentation can pose unforeseen challenges to biodiversity[5]. Fragmentation can be a natural feature of the ecosystem (for example, oceanic islands or alpine landscapes), the result of human-mediated land-use change[6] or an inherent feature of the complex spatial and temporal distribution of breeding and foraging areas of certain species (for example, migratory fish, birds and mammals and central-place foragers). In all cases, divergent effects of climate change among distant geographical areas and across trophic levels[7] impose additional constraints resulting in nonlinear responses[8]. Although correlative niche modelling has proved to be efficient in numerous cases due to its ability to implicitly include poorly understood ecological determinants, the importance of mechanistic approaches, which explicitly account for physiological or ecological processes, is increasingly recognized in ecological niche modelling[9,10]. Proper mechanistic niche modelling remains mainly restricted to ectothermal species affording accurate experimental metabolic measurements[9]. Yet, species-specific biophysical responses to climatic factors can be used in correlative models together with demographic and trophic parameters[11,12]. On a more complex level, the integration of genetic information into habitat modelling, even though extensively described[13,14], has been limited to the inclusion of phylogeography into correlative niche models[15], or to mechanistic approaches based on experimental physiology but lacking long-term validation[16]. Here, we use inference of current population connectivity and of past population size change from species-level genomic data to support and validate an ecological niche model based on biophysical constraints (that is, biophysical-ENM[12]). Integrating data on habitat distribution, trophic interactions and fitness constraints, together with dispersal abilities, population structure and palaeodemography, we provide novel insights into demographic and biogeographic response to current global warming in a species living in a complex and fragmented ecosystem.

We focus on the case of a key upper-level predator in one of the most rapidly changing ecosystems of our planet: the king penguin (*Aptenodytes patagonicus*), a central-place forager in the sub-Antarctic region, and a typical example of fragmented distribution of breeding and foraging resources. While a poleward range shift is the predicted response to climate warming for cold-adapted species[17], the highly fragmented nature of the king penguin's habitat precludes continuous population displacement. Since king penguins breed exclusively on year-round ice-free areas on islands scattered throughout the Southern Ocean, they can disperse only in a stepping-stone manner amongst the few available islands. Their foraging grounds, on the other hand, move together with the myctophid fish stock that thrives around the Antarctic Polar Front (APF)[18]. The most extensively

[1]Université de Strasbourg, Centre National de la Recherche Scientifique (CNRS), Institut Pluridisciplinaire Hubert Curien (IPHC), Strasbourg, France. [2]Département de Biologie Polaire, Centre Scientifique de Monaco (CSM), Monaco, Monaco. [3]Laboratoire International Associé (LIA-647 BioSensib, CSM-CNRS-Unistra), Monaco, Monaco. [4]Centre for Ecological and Evolutionary Synthesis (CEES), Department of Biosciences, University of Oslo, Oslo, Norway. [5]Department of Epidemiology, Human Genetics and Environmental Sciences, School of Public Health, University of Texas Health Science Center at Houston, Houston, TX, USA. [6]Centre d'Ecologie Fonctionnelle et Evolutive (CEFE), CNRS, Université de Montpellier, Université Paul-Valéry Montpellier, EPHE, Montpellier, France. [7]Centre d'Etudes Biologiques de Chizé (CEBC), CNRS-Université de La Rochelle, Villiers-en-Bois, France. [8]DST/NRF Centre of Excellence at the Percy FitzPatrick Institute for African Ornithology, Department of Zoology, Nelson Mandela University, South Campus, Port Elizabeth, South Africa. [9]Département de Biologie Marine, Centre Scientifique de Monaco (CSM), Monaco, Monaco. Present address: [10]Université Côte d'Azur, CNRS, ECOMERS, Nice, France. [11]Department of Botany and Biodiversity Research, University of Vienna, Vienna, Austria. [12]Department of Life Sciences and Biotechnology, University of Ferrara, Ferrara, Italy. [13]These authors contributed equally: Céline Le Bohec and Emiliano Trucchi. [14]These authors jointly supervised this work: Céline Le Bohec and Emiliano Trucchi. *e-mail: celine.lebohec@iphc.cnrs.fr; emiliano.trucchi@unife.it

© 2018 Macmillan Publishers Limited, part of Springer Nature. All rights reserved.

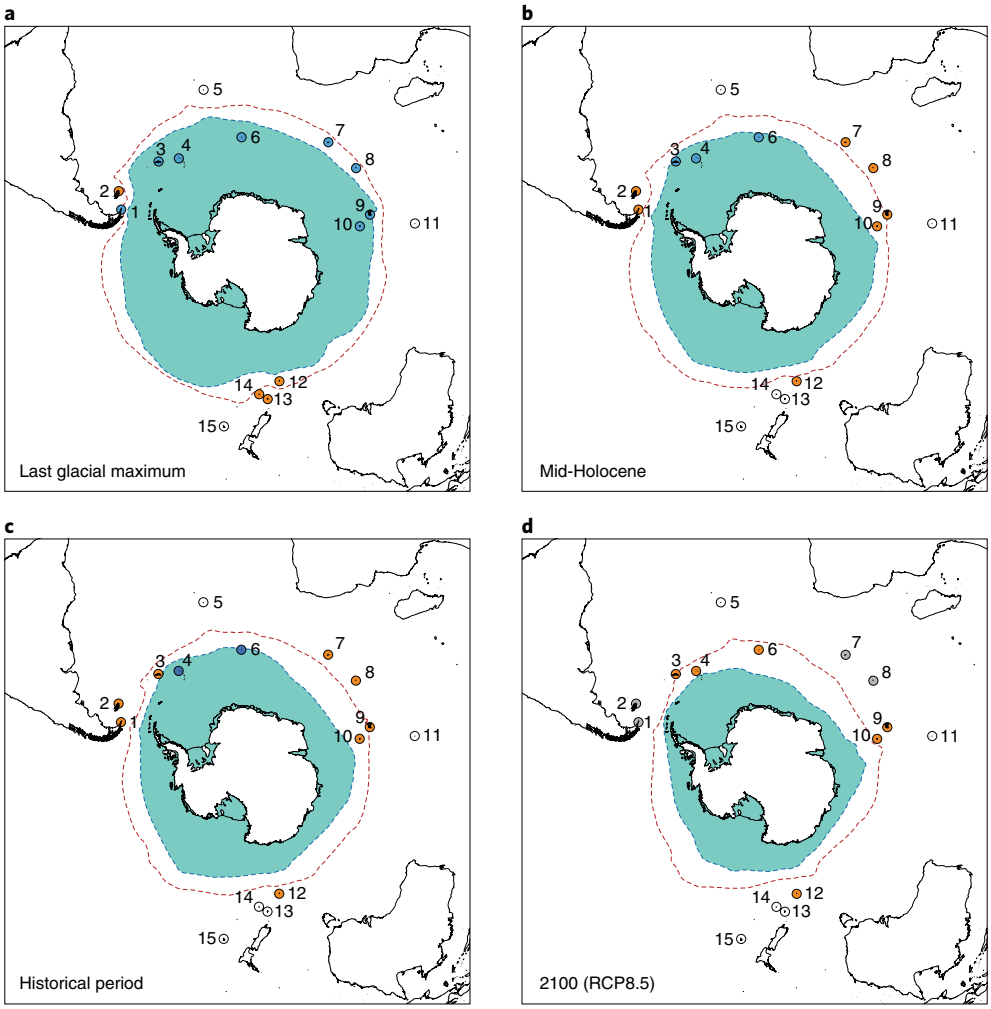

Fig. 1 | Past and future breeding range of the king penguin. a–d, Inferred position of the APF, the most important foraging ground for the king penguin, in February (sea surface temperature = 5 °C, dashed red line), and extent of sea ice in September (sea-ice concentration > 15%, light blue area) at four time periods: LGM (21–19 ka; **a**), mid-Holocene (6 ka; **b**), historical period (1981–2005; **c**), projection for 2100 according to the worst-case greenhouse gas concentration trajectory (RCP8.5; **d**). Occupation status of the islands—orange: presence of king penguin breeding colonies; blue: sea and/or land ice preventing colony foundation; grey: too far from the APF for foraging; white: never occupied by king penguin. Islands—1: Tierra del Fuego; 2: Falklands; 3: South Georgia; 4: South Sandwich; 5: Gough; 6: Bouvet; 7: Marion and Prince Edward; 8: Crozet; 9: Kerguelen; 10: Heard and McDonald; 11: Amsterdam; 12: Macquarie; 13: Auckland; 14: Campbell; 15: Chatham.

studied colony, belonging to the largest breeding concentration of the species (the Crozet archipelago), appears to have undergone tremendous growth during Holocene warming[19]. However, recent tracking studies focusing on inter-annual climatic variability have revealed a southward displacement in their foraging range in response to regional warming[18,20]. As a result of the longer foraging trips and associated increase in energy expenditure, the Crozet population is expected to decline within the coming decades[18,21]. The continuous poleward displacement of the species' foraging grounds, combined with the discrete distribution of its breeding locations, implies that king penguin populations must undergo abrupt location shifts from island to island to follow their habitat.

High dispersal prevents population structuring

Reduced dispersal ability could limit the response of a species to environmental change[22], in particular when the species presents a fragmented distribution. The lack of population structure in the king penguin, probably explained by a remarkably high migration rate among colonies, has recently been proposed[23]. To test this hypothesis and to assess the king penguin's dispersal rate, we produced a genome-wide data set including about 35,000 independent polymorphic loci genotyped in 163 individuals from 13 different locations covering most of the king penguin's contemporary range (Supplementary Fig. 1 and Supplementary Table 1). Analyses of this extensive data set clearly support the existence of a single, well-mixed genetic pool, and contradict the alleged separation between the South Atlantic *A. p. patagonicus* and the South Indian and Pacific *A. p. halli* subspecies[24], suggesting that the traits used as a basis for subspecies delineation are better explained by phenotypic plasticity than by reproductive isolation. Both classical descriptors of genetic variation and structure analysis unambiguously support a well-mixed worldwide population (see the Analysis of genetic data section in the Methods, Supplementary Table 2 and Supplementary Notes 2.1–2.5). Complete admixture among colonies is also clear when repeating these analyses at the island level (see Methods). The recent population expansion following human overexploitation may explain part of this admixture, although previous studies did not detect a bottleneck signature in heavily affected Macquarie island[25]. Moreover, bio-logging experiments and empirical observations show short- and long-distance movements as significant contributors to the ongoing genetic mixing. In contrast to previous hypotheses, recapture of tagged

© 2018 Macmillan Publishers Limited, part of Springer Nature. All rights reserved.

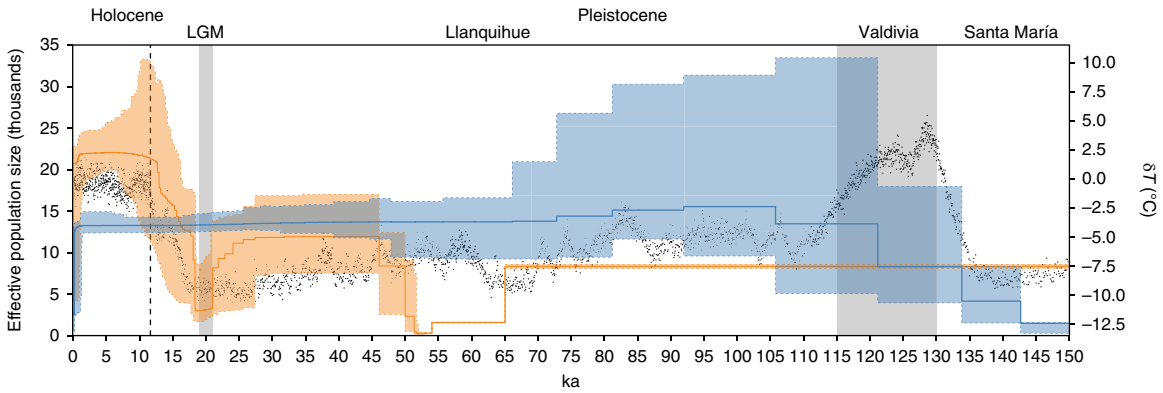

Fig. 2 | King and emperor penguins' past demography in response to Quaternary climate change. Reconstruction of population size changes (left *y* axis) from the last interglacial to the present time for the king penguin (orange) and the emperor penguin (blue). Solid line: median population size; shaded area: 95% confidence interval. The temperature anomaly in the late Quaternary (black dots, right *y* axis), as inferred from the EPICA (European Project for Ice Coring in Antarctica) Dome C ice core[51], is shown. Highlighted areas: LGM (~21–19 ka) and Valdivian interglacial period (~130–115 ka). Dashed line: Pleistocene–Holocene transition (~11.7 ka). Data for the emperor penguin are from ref. [36].

individuals up to about 1,400 km away shows that dispersal is also strong at the generation scale (see Supplementary Note 3). While such observations do not directly demonstrate breeding dispersal (most detections lack information as to breeding status), they do indicate the capacity of king penguins to explore new habitats during their lifetime. In addition, new colonies have been established in the past decades, most likely fuelled by immigration[26,27]. Thus, we can assume that dispersal ability is not a limiting factor in the king penguin's response to environmental change and cryptic genetic structure is unlikely to be a confounding factor in population genomic analyses, a rare advantage for worldwide population studies[28].

Past demography supports the biophysical-ENM

The king penguin's response to climate change can be explained by modelling the variations in the extent of both breeding and foraging suitable habitats. The high trophic level of this species, which makes it a sensitive indicator of environmental change[21], and its complex discontinuous distribution of breeding and foraging grounds severely limit the use of traditional correlative models based on occurrence data[29]. As well-characterized physiological responses to climate-related factors are known to constrain the king penguin's range, a biophysical ecological niche model that accounts for such traits should better represent its fundamental niche[12]. Our model was thus defined using three major biophysical constraints that directly determine habitat suitability for the species. We considered that a breeding colony in the Southern Ocean can exist only if: there is insular (that is, predator-free) and ice-free land[24]; the island is within the maximum foraging distance of the prey stock at the APF[30] (the duration of the parent's foraging trip cannot exceed the offspring's resistance to starvation); there is low sea-ice concentration around the island during winter, allowing access to open waters for over-winter chick-rearing[24]. Taken together, these three binary requirements define a grid through which locations in the Southern Ocean are scored as suitable or unsuitable. From available climate models (see the Environmental data section in the Methods), we extracted the sea surface temperature to model the APF position and its distance from each sub-Antarctic island (see the Assessment of the APF location section in the Methods) and the sea-ice concentration to model winter sea ice around each island (see the Assessment of winter sea-ice concentration section in the Methods). Although the global productivity of the Southern Ocean can be assumed to be constant throughout the Quaternary period[31,32], the same cannot be said of its spatial structure. The location of the APF zone and the extent of land-ice and winter sea-ice cover exhibited important latitudinal variation during these periods[32–34]. As a consequence, the location of optimal king penguin breeding areas changed vastly between warm and cold conditions. APF and foraging range predictions, based on historical period (1981–2005) experiments from an ensemble of 15 atmosphere–ocean climate models, closely matched both observed APF and empirical foraging distances derived from bio-logging experiments (see Methods and Supplementary Notes 4 and 5).

Our model is able to capture the full present-day range of the king penguin (Fig. 1c). However, its validation for future habitat projections requires knowledge of its stability over long time periods[14]. We therefore verified that our model was also able to explain the long-term relationship between palaeohabitat reconstructions and the species' past demography inferred from genomic data (Figs. 1a,b and 2). We reconstructed king penguin past demography applying a novel approach (the Stairway plot[35] calculated from the genomic data set described above). This approach was compared to two different Bayesian analyses performed on a subset of the data and on three additional whole-genome sequences, respectively, and further validated through simulations (see the Demographic reconstructions section in the Methods and Supplementary Notes 2.6–2.9 for details). According to our reconstruction, the king penguin population experienced two bottlenecks: a recent one during the Last Glacial Maximum (LGM: 21–19 thousand years ago (ka)) and a more ancient one overlapping with the previous Pleistocene glacial 'Llanquihue' episode (Fig. 2). During the late Pleistocene and early Holocene (about 17–10 ka), a period of steep population growth is followed by a long plateau. These analyses were repeated for the emperor penguin, based on available data[36] and on additional whole-genome sequences of three individuals produced in the present study (see the Demographic reconstructions section in the Methods and Supplementary Note 2.6–2.9). The large fluctuations that we observe in the king penguin population are not mirrored in the emperor penguin (Fig. 2). This observation supports the view that the overall productivity of the Southern Ocean did not change significantly during the Pleistocene and Holocene periods[31,32], and allows us to reject the hypothesis that large changes in primary productivity, rather than habitat suitability as we define it, are the proximal cause of king penguin population size changes.

Under LGM conditions, the equatorward displacement of the APF and increased land- and sea-ice cover[32,34] reduced the king penguin's range to a fraction of its current extent (Fig. 1a,c), as suggested by the

© 2018 Macmillan Publishers Limited, part of Springer Nature. All rights reserved.

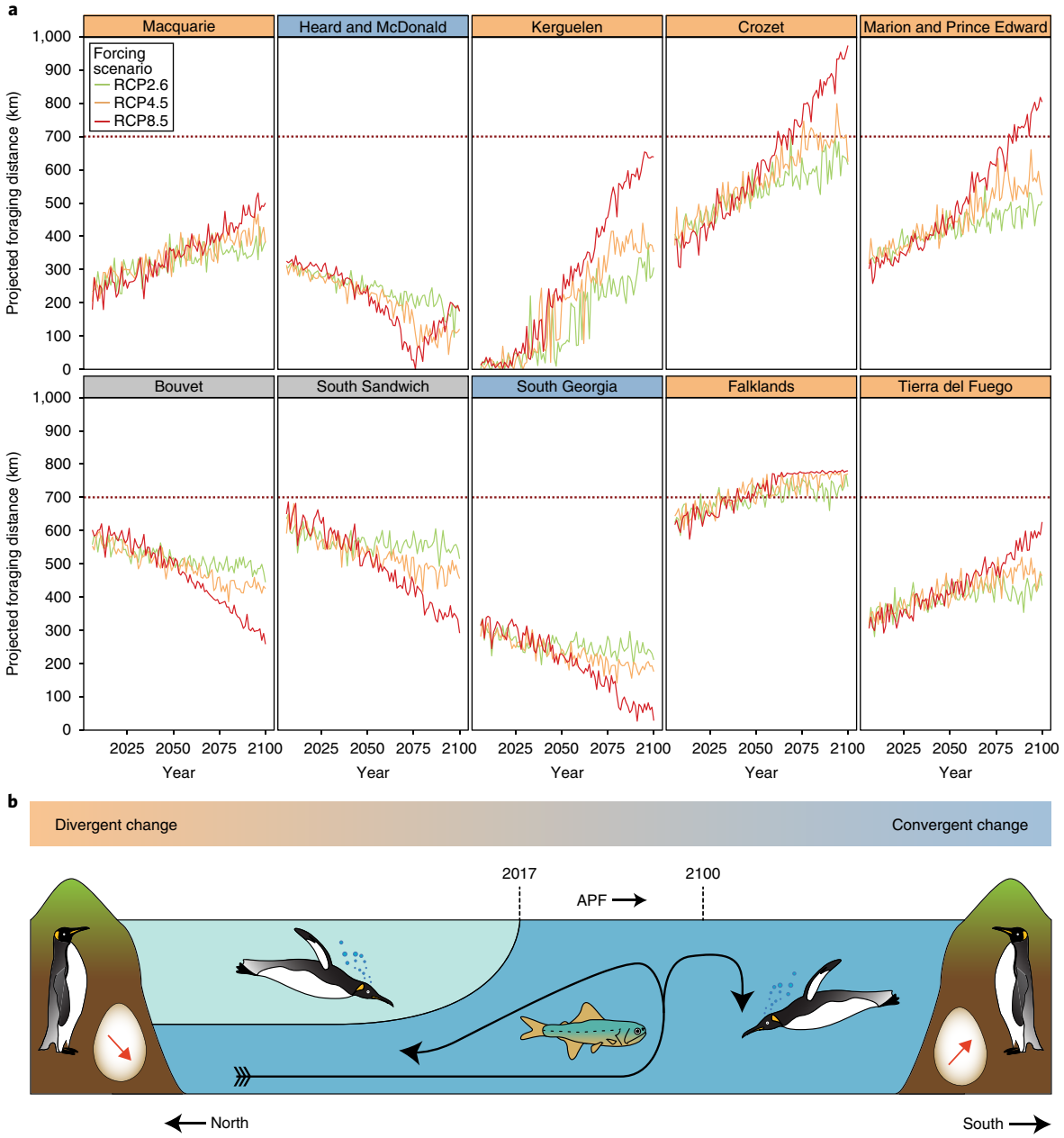

Fig. 3 | Convergent and divergent effects of climate change. Climate change effects. a, Projected foraging distance under three greenhouse gas concentration scenarios. The mean projected summer foraging distances for the king penguin from eight currently occupied archipelagos (see Supplementary Fig. 1) and two possible future breeding archipelagos (Bouvet and South Sandwich) are shown. The foraging distances are estimated using 15 global coupled atmosphere–ocean general circulation models (from the Coupled Model Intercomparison Project Phase 5 (CMIP5)), over the twenty-first century, under three different greenhouse gas concentration trajectories: RCP2.6, RCP4.5 and RCP8.5. Horizontal red line: 700 km limit, beyond which no successful breeding of king penguin is expected. The locality name is highlighted according to increasing (orange) or decreasing (blue) distance to the foraging grounds at the APF; localities in grey are not yet occupied by the king penguin. According to the worst-case scenario (RCP8.5), king penguin colonies are predicted to disappear from Crozet and Prince Edward, undergo significant population decline (or disappear) in Kerguelen and newly colonized Tierra del Fuego, remain unchanged in Macquarie Island, grow on South Georgia and Heard, and settle on Bouvet, and possibly the South Sandwich, as the winter sea ice disappears (see Fig. 2). According to low-to-medium-warming scenarios (RCP2.6 and RCP4.5, respectively), only Crozet and Prince Edward are too far from the foraging grounds to sustain large breeding colonies by 2100, while Kerguelen remains in a favourable situation. **b**, Schematic representation of the different results of climate change in the Southern Ocean. Dark and light water masses: cold Antarctic deep water and warmer sub-Antarctic surface water (major circulation as a black arrow). Dashed lines: position of the APF in 2015 and 2100 (the APF is shifting southward). The red arrows in the eggs represent the trend in breeding success. Longer foraging trips from the colony to the APF decrease the breeding success (divergent change, orange) while shorter trips have the opposite effect (convergent change, blue).

inferred population bottleneck (Fig. 2). Assuming a 700-km February foraging distance as the upper limit for successful breeding[20], the only two possible refugia were found in the Falklands, and in the Campbell Plateau region, a much reduced range compared to the eight pre-industrial breeding areas[37]. The main islands of New Zealand, on the other hand, would have remained too far removed from the APF due

© 2018 Macmillan Publishers Limited, part of Springer Nature. All rights reserved.

to the configuration of the Campbell Plateau, while the presence of large, mainly canid predators, absent at that time from the Falklands[38], would have prevented colony formation in mainland Patagonia. By the mid-Holocene (6 ka), on the other hand, the king penguin already occupied most of its pre-industrial range (Fig. 1b,c). The APF occupied a position close to its present-day state at most locations, while all present-day breeding archipelagos (except for South Georgia) were free from sea ice. Land ice receded early on Kerguelen and South Georgia—although it persisted until the early Holocene on Crozet and Prince Edward archipelagos[34]. The king penguin rapidly exploited these newly available locations, as suggested by the steep growth and the following plateau in our demographic reconstructions (Fig. 2). Thus, the king penguin's response to past climate change clearly supports the idea that modifications in the position of the APF and in the distribution of land and sea ice, by modifying the extent of available habitat, have a major impact on the species' demographic trajectory.

Forecasting king penguin future distribution

The validation of our model across the past ~25 ka supports its application to near-future scenarios. Projected changes for the twenty-first century are expected to have a deep impact on the king penguin's range and population size. The uncoupled trends in the mobile food resources of the APF and the static breeding locations may have opposite effects depending on the initial state (Figs. 1d and 3, and Supplementary Figs. 8 and 9): foraging distance increases steadily until the end of the century for the world's largest colonies, located north of the APF (divergent change); conversely, conditions become more favourable on the colder archipelagos south of the APF, with shorter foraging distances and decreased sea ice (convergent change). Although variability among different climatic scenarios is relatively high (see the Uncertainty assessment of the modelling approach section in the Methods), the trend is consistent across individual models (Fig. 3 and and Supplementary Note 5) and supported by three different greenhouse gas concentration trajectory forcing scenarios (Representative Concentration Pathways $+2.6\,W\,m^{-2}$, RCP2.6; $+4.5\,W\,m^{-2}$, RCP4.5; and $+8.5\,W\,m^{-2}$, RCP8.5)[39]. Even if the specific composition of the abundant food source required for colony persistence may change, this food source is oceanographically bound to be displaced together with the primary productivity area of the APF upwelling[40], as it cannot be sustained by the lower-productivity sub-Antarctic convergence[41] or local shelf-break areas[42]. Due to its low genetic diversity and long generation time, the species is not expected to undergo rapid adaptive evolution to the new conditions at the northern end of its range[43,44] and changes in foraging strategy may arise only from behavioural plasticity. Local extinction or dispersal, rather than adaptation, is therefore the predicted outcome.

Colony loss is likely to bring about a decrease in population size, although high dispersal ability also implies that newly available locations may be colonized rapidly. Under the 'business-as-usual' RCP8.5 scenario, 70% of the present-day 1.6 million king penguin breeding pairs[37] are expected to abruptly relocate or disappear before the end of the century (Figs. 1d and 3a): 49% of the world population are projected to lose their habitat completely (on Crozet and Prince Edward), and 21% will probably see their habitat strongly altered due to regularly near-limit foraging distances (on Kerguelen, the Falklands and Tierra del Fuego). These losses may be partly compensated by the predicted colonization of Bouvet, and by a possible additional growth on Heard and South Georgia due to improved foraging conditions (Figs. 1d and 3a). These last two locations, together with Macquarie Island, are likely to become the major cold refugia for the king penguin in the coming decades. Under the low-emission RCP2.6 scenario, only Crozet and Falkland populations come under direct threat, while other colonies may retain good foraging conditions (Fig. 3a and Supplementary Figs. 8 and 9), and undergo minimal demographic impact. Thus, our results stress the importance of immediate action to avoid the catastrophic RCP8.5 scenario, as efficient attenuation strategies may still have a positive outcome for the Southern Ocean biodiversity. We also insist on the importance of taking proactive conservation measures in areas of the Southern Ocean that, like Bouvet, may act as cold biodiversity refugia for forthcoming warm-Earth conditions[45].

Our findings clearly predict a severe disruption in the geographical distribution of the king penguin, an emblematic umbrella species[46]. Our projection is, furthermore, likely to be an underestimate, as we take into account only the maximum foraging distance after which no successful breeding is expected to take place. However, increasing foraging distances, even if below the 700-km limit, have been shown to affect breeding success strongly, and may trigger a colony decrease well before the extinction threshold is reached[18,21]. Although this limit derives from long-term observations in the Crozet archipelago alone[20], we consider it unlikely that either adult travelling speed or offspring fasting abilities vary locally, given the lack of genetic differentiation across the species' range. In addition, our model does not take into account aggravating effects of climate change, such as sea-level rise or a decrease in ocean productivity due to ocean acidification[47] and reduction of the global thermohaline circulation[48]. The abrupt nature of the predicted range shift may also accelerate the restructuring and concentration of biotic interactions (for example, range overlap and competition with other penguin species) generating complex feedback effects not included in our model. Finally, climate change might also modify the nature of the prey available to the king penguin, through its impact on oceanic features and trophic networks of the Southern Ocean, with unpredictable consequences on their diet and thus on the outcome of the models.

Conclusions

Many species are naturally or artificially constrained into fragmented habitats where the effects of climate change can be enormously exacerbated[49,50]. The king penguin's complex stepping-stone trajectory offers a paradigmatic representation of the impact of global warming on species' distributions whenever heterogeneous environmental changes lead to uncoupled effects on different critical areas—for example, breeding, foraging or overwintering grounds. In such contexts, reliable species' distribution modelling is an indispensable tool to foresee the effects of climate change and take preventive measures for biodiversity conservation[13]. Our modelling approach successfully integrates genetic-based demographic inference[13], so far mostly restricted to phylogeography (for example, leading to the prediction of the grey whale's reappearance in the Atlantic[15]), or to functional genomics (for example, predicting future hotspots for dengue-carrying mosquitoes in Australia[16]), and well-characterized biophysical constraints[12]. This allowed us to directly link range and demographic responses to environmental conditions in the common situation where accurate experimental physiological measurements are impossible. When habitat-limiting factors are known, a similar operative framework can be applied in all of those cases where complex uncoupled effects make traditional correlative niche models less reliable; for example, where natural or anthropogenic habitat fragmentation increases the risk of divergent trends in the different portions of a species' niche[4], or generally whenever the adaptability of a species to habitat changes is made unclear by complex biotic interactions[14]. As the paradigmatic example of the king penguin clearly shows, integrating the total available evidence for a species offers unexpected insights into future scenarios in complex ecosystems identifying vulnerable areas and potential refugia, and allowing for efficient and proactive conservation efforts.

Methods

Methods, including statements of data availability and any associated accession codes and references, are available at https://doi.org/10.1038/s41558-018-0084-2.

© 2018 Macmillan Publishers Limited, part of Springer Nature. All rights reserved.

Received: 16 February 2017; Accepted: 19 January 2018;
Published online: 26 February 2018

References

1. Thomas, C. D. et al. Extinction risk from climate change. *Nature* **427**, 145–148 (2004).
2. Pacifici, M. et al. Assessing species vulnerability to climate change. *Nat. Clim. Change* **5**, 215–224 (2015).
3. Charmantier, A. et al. Adaptive phenotypic plasticity in response to climate change in a wild bird population. *Science* **320**, 800–803 (2008).
4. Garcia, R. A., Cabeza, M., Rahbek, C. & Araújo, M. B. Multiple dimensions of climate change and their implications for biodiversity. *Science* **344**, 1247579 (2014).
5. Walther, G.-R. et al. Ecological responses to recent climate change. *Nature* **416**, 389–395 (2002).
6. Gouveia, S. F. et al. Climate and land use changes will degrade the configuration of the landscape for titi monkeys in eastern Brazil. *Glob. Change Biol.* **22**, 2003–2012 (2016).
7. Edwards, M. & Richardson, A. J. Impact of climate change on marine pelagic phenology and trophic mismatch. *Nature* **430**, 881–884 (2004).
8. Saraux, C. et al. Reliability of flipper-banded penguins as indicators of climate change. *Nature* **469**, 203–206 (2011).
9. Kearney, M. & Porter, W. Mechanistic niche modelling: combining physiological and spatial data to predict species' ranges. *Ecol. Lett.* **12**, 334–350 (2009).
10. Thuiller, W. et al. A road map for integrating eco-evolutionary processes into biodiversity models. *Ecol. Lett.* **16**, 94–105 (2013).
11. Elith, J., Kearney, M. & Phillips, S. The art of modelling range-shifting species. *Methods Ecol. Evol.* **1**, 330–342 (2010).
12. Fordham, D. A. et al. Population dynamics can be more important than physiological limits for determining range shifts under climate change. *Glob. Change Biol.* **19**, 3224–3237 (2013).
13. Fordham, D. A., Brook, B. W., Moritz, C. & Nogués-Bravo, D. Better forecasts of range dynamics using genetic data. *Trends Ecol. Evol.* **29**, 436–443 (2014).
14. Fordham, D. A. et al. Predicting and mitigating future biodiversity loss using long-term ecological proxies. *Nat. Clim. Change* **6**, 909–916 (2016).
15. Alter, S. E. et al. Climate impacts on transocean dispersal and habitat in gray whales from the Pleistocene to 2100. *Mol. Ecol.* **24**, 1510–1522 (2015).
16. Kearney, M., Porter, W. P., Williams, C., Ritchie, S. & Hoffmann, A. A. Integrating biophysical models and evolutionary theory to predict climatic impacts on species' ranges: the dengue mosquito in Australia. *Funct. Ecol.* **23**, 528–538 (2009).
17. Chen, I.-C., Hill, J. K., Ohlemüller, R., Roy, D. B. & Thomas, C. D. Rapid range shifts of species associated with high levels of climate warming. *Science* **333**, 1024–1026 (2011).
18. Bost, C. A. et al. Large-scale climatic anomalies affect marine predator foraging behaviour and demography. *Nat. Commun.* **6**, 8220 (2015).
19. Trucchi, E. et al. King penguin demography since the last glaciation inferred from genome-wide data. *Proc. R. Soc. B* **281**, 20140528 (2014).
20. Péron, C., Weimerskirch, H. & Bost, C.-A. Projected poleward shift of king penguins' (*Aptenodytes patagonicus*) foraging range at the Crozet Islands, southern Indian Ocean. *Proc. R. Soc. B* **279**, 2515–2523 (2012).
21. Le Bohec, C. et al. King penguin population threatened by Southern Ocean warming. *Proc. Natl Acad. Sci. USA* **105**, 2493–2497 (2008).
22. Engler, R. et al. Predicting future distributions of mountain plants under climate change: does dispersal capacity matter. *Ecography* **32**, 34–45 (2009).
23. Clucas, G. V. et al. Dispersal in the sub-Antarctic: king penguins show remarkably little population genetic differentiation across their range. *BMC Evol. Biol.* **16**, 211 (2016).
24. Barrat, A. Quelques aspects de la biologie et de l'écologie du manchot royal *Aptenodytes patagonicus* des îles Crozet. *Com. Natl Fr. Rech. Antarct.* **40**, 9–51 (1976).
25. Heupink, T. H., van den Hoff, J. & Lambert, D. M. King penguin population on Macquarie Island recovers ancient DNA diversity after heavy exploitation in historic times. *Biol. Lett.* **8**, 586–589 (2012).
26. Pistorius, P. A., Baylis, A., Crofts, S. & Pütz, K. Population development and historical occurrence of king penguins at the Falkland Islands. *Antarct. Sci.* **24**, 435–440 (2012).
27. Kusch, A. & Marín, M. Sobre la distribución del Pingüino Rey Aptenodytes Patagonicus (Aves: *Spheniscidae*) en Chile. *An. Inst. Patagonia* **40**, 157–163 (2012).
28. Wallberg, A. et al. A worldwide survey of genome sequence variation provides insight into the evolutionary history of the honeybee *Apis mellifera*. *Nat. Genet.* **46**, 1081–1088 (2014).
29. Pearson, R. G. & Dawson, T. P. Predicting the impacts of climate change on the distribution of species: are bioclimate envelope models useful? *Glob. Ecol. Biogeog.* **12**, 361–371 (2003).
30. Bost, C.-A. et al. The importance of oceanographic fronts to marine birds and mammals of the southern oceans. *J. Mar. Syst.* **78**, 363–376 (2009).
31. Wolff, E. W. et al. Southern Ocean sea-ice extent, productivity and iron flux over the past eight glacial cycles. *Nature* **440**, 491–496 (2006).
32. Kohfeld, K. E. et al. Southern Hemisphere westerly wind changes during the Last Glacial Maximum: paleo-data synthesis. *Quat. Sci. Rev.* **68**, 76–95 (2013).
33. Gersonde, R., Crosta, X., Abelmann, A. & Armand, L. Sea-surface temperature and sea ice distribution of the Southern Ocean at the EPILOG Last Glacial Maximum: a circum-Antarctic view based on siliceous microfossil records. *Quat. Sci. Rev.* **24**, 869–896 (2005).
34. Hodgson, D. A. et al. Terrestrial and submarine evidence for the extent and timing of the Last Glacial Maximum and the onset of deglaciation on the maritime-Antarctic and sub-Antarctic islands. *Quat. Sci. Rev.* **100**, 137–158 (2014).
35. Liu, X. & Fu, Y.-X. Exploring population size changes using SNP frequency spectra. *Nat. Genet.* **47**, 555–559 (2015).
36. Cristofari, R. et al. Full circumpolar migration ensures evolutionary unity in the Emperor penguin. *Nat. Commun.* **7**, 11842 (2016).
37. Borboroglu, P. G. & Boersma, P. D. *Penguins: Natural History and Conservation* (University of Washington Press, Seattle & London, 2013).
38. Austin, J. J. et al. The origins of the enigmatic Falkland Islands wolf. *Nat. Commun.* **4**, 1552 (2013).
39. Meinshausen, M. et al. The RCP greenhouse gas concentrations and their extensions from 1765 to 2300. *Clim. Change* **109**, 213–241 (2011).
40. Carr, M.-E. et al. A comparison of global estimates of marine primary production from ocean color. *Deep Sea Res. II* **53**, 741–770 (2006).
41. Froneman, P. W., Laubscher, R. K. & McQuaid, C. D. Size-fractionated primary production in the south Atlantic and Atlantic sectors of the Southern Ocean. *J. Plankton Res.* **23**, 611–622 (2001).
42. Pütz, K. & Cherel, Y. The diving behaviour of brooding king penguins (*Aptenodytes patagonicus*) from the Falkland Islands: variation in dive profiles and synchronous underwater swimming provide new insights into their foraging strategies. *Mar. Biol.* **147**, 281–290 (2005).
43. Hoffmann, A. A. & Sgrò, C. M. Climate change and evolutionary adaptation. *Nature* **470**, 479–485 (2011).
44. Norberg, J., Urban, M. C., Vellend, M., Klausmeier, C. A. & Loeuille, N. Eco-evolutionary responses of biodiversity to climate change. *Nat. Clim. Change* **2**, 747–751 (2012).
45. Hope, A. G., Waltari, E., Payer, D. C., Cook, J. A. & Talbot, S. L. Future distribution of tundra refugia in northern Alaska. *Nat. Clim. Change* **3**, 931–938 (2013).
46. Roberge, J. M. & Angelstam, P. Usefulness of the umbrella species concept as a conservation tool. *Conserv. Biol.* **18**, 76–85 (2004).
47. Jackson, J. B. C. Ecological extinction and evolution in the brave new ocean. *Proc. Natl Acad. Sci. USA* **105**, 11458–11465 (2008).
48. Kuhlbrodt, T. et al. An integrated assessment of changes in the thermohaline circulation. *Clim. Change* **96**, 489–537 (2009).
49. Travis, J. M. Climate change and habitat destruction: a deadly anthropogenic cocktail. *Proc. R. Soc. B* **270**, 467–473 (2003).
50. Ewers, R. M. & Didham, R. K. Confounding factors in the detection of species responses to habitat fragmentation. *Biol. Rev.* **81**, 117–142 (2006).
51. Augustin, L. et al. Eight glacial cycles from an Antarctic ice core. *Nature* **429**, 623–628 (2004).

Acknowledgements

This work was conducted within the framework of the Programme 137 of the Institut Polaire Français Paul-Emile Victor (IPEV; CLB), with additional support from the French National Research Agency (ANR) 'PICASO' grant (ANR-2010-BLAN-1728-01; Y.L.M.), Marie Curie Intra European Fellowships (FP7-PEOPLE-IEF-2008, European Commission; project no. 235962 to C.L.B. and FP7-PEOPLE-IEF-2010, European Commission; project no. 252252 to E.T.), the Centre Scientifique de Monaco through the budget allocated to the Laboratoire International Associé 647 *BioSensib* (CSM/CNRS-University of Strasbourg; C.L.B., Y.L.M.), the Centre National de la Recherche Scientifique (Programme Zone Atelier de Recherches sur l'Environnement Antarctique et Subantarctique), South African National Antarctic Programme (P.P.) and the IPEV Programme 109 (Y.C.). Logistic and field costs of research were supported by the IPEV Programme 137 (C.L.B.), the South African Department of Environmental Affairs and the National Research Foundation (P.P.). This work was performed on the Abel Cluster, owned by the University of Oslo and the Norwegian Metacenter for High Performance Computing (NOTUR), and operated by the Department for Research Computing at USIT, the University of Oslo. We are very grateful to M. Skage, A. Tooming-Klunderud, M. Selander-Hansen and the Norwegian Sequencing Center for their very valuable help in the laboratory, as well as L. Nederbragt and M. Matschiner for their assistance with the Abel cluster, and M. Fumagalli and T. Korneliussen for their precious advice regarding ngsTools and ANGSD. We thank G. Bertorelle, L. Fusani, A. Mazzarella and D. Fordham for useful comments and advice. We acknowledge the World Climate Research Programme's Working Group on Coupled Modelling, which is responsible for CMIP, and we thank the climate modelling groups (listed in Supplementary Table 1) for producing and making available their model output. For CMIP, the US Department of Energy's

© 2018 Macmillan Publishers Limited, part of Springer Nature. All rights reserved.

Program for Climate Model Diagnosis and Intercomparison provides coordinating support and led development of software infrastructure in partnership with the Global Organization for Earth System Science Portals.

Author contributions

C.L.B. and E.T. conceived and supervised the study. C.L.B., F.B., Y.C. and P.P. collected the samples. R.C. performed DNA extraction, library preparation, and prepared and performed the genomic and demographic analyses and the climate modelling. X.L. and E.T. participated in the genomic and demographic analyses. V.R. and C.L.B. participated in climate modelling. N.C.S. hosted the project. R.C., C.L.B. and E.T. wrote the manuscript. F.B., N.C.S., P.P., Y.C., Y.L.M. and V.R. commented the manuscript.

Competing interests

The authors declare no competing interests.

Additional information

Supplementary information is available for this paper at https://doi.org/10.1038/s41558-018-0084-2.

Reprints and permissions information is available at www.nature.com/reprints.

Correspondence and requests for materials should be addressed to C.L. or E.T.

Publisher's note: Springer Nature remains neutral with regard to jurisdictional claims in published maps and institutional affiliations.

© 2018 Macmillan Publishers Limited, part of Springer Nature. All rights reserved.

Methods

From sample collection to SNP typing. Between 2010 and 2014, 163 king penguin blood samples were collected (from fledged juveniles or breeding adults), on 13 colonies covering most of the species' range (Supplementary Fig. 1 and Supplementary Table 1). DNA extraction, single-digest restriction-site-associated DNA (RAD)-sequencing, sequence demultiplexing, read mapping and filtering followed a previously published protocol[36]. All sites that were identified as belonging to coding regions[52], or to sex chromosomes[53], were excluded from the analysis. For single-nucleotide polymorphism (SNP)-based analysis, joint SNP and genotype calling was performed using the GATK HaplotypeCaller pipeline[54] with standard parameters, except for population heterozygosity, which was set to 0.01. Depending on analysis requirements, we retained: SNPs genotyped in at least 90% individuals (~60,000 sites, data set A1); SNPs with a minimum depth of coverage of 4×, and minimum sample representation of 80% (~4,700 sites, data set A2); or unlinked variable RAD loci with 1 to 6 SNPs (~12,000 loci, data set A3). ANGSD 0.9008[55] was used to compute the per-site probability of being variable, retaining only highly probable polymorphisms (~150,000 sites, *P* value threshold 1×10^{-6}). We extracted genotype posterior probabilities (data set B1), and raw genotype likelihoods (data set B2), using the Samtools mpileup/bcftools algorithm, and the complete sample allele frequency information as a prior. Per-site allele-frequency likelihood distribution was used to produce a maximum-likelihood (ML) estimate of the derived allele frequency spectrum, either unidimensional at the population or species level, or a pairwise joint spectrum between pairs of populations. To polarize allele-frequency spectra, we reconstructed the most likely ancestral base for all positions in the RADome. On the basis of 12 king penguin and 12 emperor penguin samples covering the whole species' ranges[36], and using only high-quality polymorphisms (phred-scale genotype quality ≥ 80), we reconstructed the ancestral sequence for crown-*Aptenodytes* in PhyML[56], PAML[57] and Lazarus[58], using the Adélie penguin genome (*Pygoscelis adeliæ*[52]) as an outgroup. In addition, we selected three high-quality samples for the king penguin, and three for the emperor penguin to perform whole-genome re-sequencing. Libraries were prepared with a standard Illumina(c) TruSeq PCR-free protocol, and multiplexed on two lanes of a HiSeq 2500 V4 sequencer at the NSC facility, University of Oslo. Reads were mapped using Bowtie2[59] to the published emperor penguin genome[52] with high success (unique concordant alignment rate, king penguin: ~86%, emperor penguin: ~81%). We retained only scaffolds with length ≥ 2 Mb (that is, 188 scaffolds making up ~80%—1,009,159,582 base pairs—of the total reference length) for the analysis.

Analysis of genetic data. Summary statistics were calculated in Arlequin 3.5.2.1[60] and with custom R scripts from data sets A1 and A3. Reich's estimator of the pairwise fixation index (F_{ST})[61] is close to zero (mean pairwise F_{ST} 0.0132 ± 0.00567). Nucleotide diversity π and Tajima's *D* were calculated from a random haploid subset to avoid possible biases due to low coverage. Tajima's *D* is slightly negative and homogeneous across locations and nucleotide diversity is low (Supplementary Table 2), in keeping with the prediction for long-lived species[62]. Principal component analysis (PCA) was performed in ngsTools[63] on data set B1 and repeated in the R package adegenet[64] on data set A2. PCA does not resolve strong geographical structure (Supplementary Fig. 2): although samples tend to gather by archipelago, there is considerable overlap between locations, and no single principal component explains more than ~0.9% of the total variation. Clustering analysis was done in ngsAdmix[65] on data set B2, with 100 bootstrap replicates and *K* values ranging from 1 to 10, and repeated in FastStructure[66] using data set A2. Both approaches unambiguously supported a $K=1$ model. The best-fitting *K* was chosen using Evanno's δK method. Analysis of molecular variance was performed in Arlequin on data set A1. Analysis of molecular variance was performed on a per-locus basis, with 10,000 permutations. We tested four different grouping schemes: colonies grouped by archipelago, *A. p. patagonicus* versus *A. p. halli*, within Crozet alone, and within Marion alone. Under all four groupings, the overwhelming majority of variance is explained at the individual level. We calculated the pairwise Hamming distance between individuals using PLINK v1.9[67] and data set A1, and calculated the corresponding neighbour-net in SplitsTree[68] (Supplementary Fig. 3A). In keeping with the results of the analysis of molecular variance and PCA, the terminal branches explain most of the variance, and samples do not cluster geographically.

Comparison of mitochondrial hypervariable control region (HVR) haplotypes from Crozet[19] (from 139 individuals, Genbank accession number KF530582-KF530621) with published sequences from Macquarie Island[25] (35 individuals, Genbank accession number JQ256379-JQ256413) confirms the idea of a single, worldwide and fully panmictic population. Pairwise F_{ST} is low ($F_{ST}=0.032$), and a haplotype network does not support any population separation between the two islands (Supplementary Fig. 3B), in keeping with recent findings[23].

Demographic reconstructions. The stairway plot is a novel model-flexible method for demographic inference[35] that relies on the maximization of the composite likelihood of the observed derived-allele frequency spectrum (DAFS), without a prior hypothesis on demographic history, as opposed to previous spectrum-based demographic inference methods[69]. ML estimation of the DAFS was performed in ANGSD-0.901 under a SAMtools model, for 140 high-quality king penguin samples, and 90 high-quality emperor penguin samples, using 2,300,996 sites. The analysis was run with 500 bootstrap replicates. Singletons were found to be the least robustly estimated frequency class, due, in particular, to the confounding effect of sequencing errors, and were consequently masked from the reconstructions, although comparison of reconstructions, including all frequency categories, excluding singletons, or excluding singletons and doubletons, shows that only the reconstruction of the most recent demographic events is affected by the low-frequency variants (Supplementary Fig. 4A–C). Similarly, using only a randomly picked subset of half of the individuals did not affect the reconstructions (Supplementary Fig. 4D). In long-lived species, the generation time is not a fixed parameter, but a function of the demographic trend. An estimator has been defined previously[70] as

$$\alpha+\frac{S}{\lambda-S}$$

where α is the female age at first breeding, *S* is the yearly adult survival rate and λ is the yearly growth rate of the population. Using long-term monitoring data for 400 adults of known age, we extracted both yearly growth rate and adult survival for the 1999–2010 period. *S* and λ were found to be strongly correlated (intercept: −0.2454, slope: 1.0936, coefficient of determination $R^2=0.6$); therefore, we extended that empirical relationship to our reconstruction. For each generation, the generation time in years was defined as

$$T_{t+1}=\alpha+\frac{S_t}{\lambda_t-S_t}$$

where λ_t and S_t are the growth rate and adult survival rate for the previous generation, with

$$\lambda_t=\left(\frac{N_{t+1}}{N_t}\right)e^{\frac{1}{T_t}}$$

where N_{t+1} and N_t are the population sizes at generations $t+1$ and T_t is the generation time in years at generation *t* and S_t is a linear function of λ_t, using empirically derived parameters. This correction was applied recursively from the oldest generation in the reconstruction assuming $\lambda=1$, and towards the present. To calibrate other analyses, the mean generation time over the whole reconstruction $T=10.6$ years was retained.

We performed a joint analysis of mitochondrial HVR and RAD data in a multilocus Extended Bayesian Skyline Plot (EBSP) framework, using the robustly established substitution rate for the Adélie penguin HVR (in substitutions per site per million years: median = 0.55, 95% confidence interval = 0.29–0.88)[71] as a calibration. Since the generation time differs widely between the Adélie penguin (6.46 years) and the king penguin (10.6 years, see above), we converted that rate to reflect the difference in generation time, to 0.34 substitutions per site per million years (95% confidence interval = 0.18–0.54). We followed a previously published protocol[36], downsampling the data to haploid individuals, and using 50 haplotypes from 50 randomly selected unlinked RAD with 3 to 6 polymorphic sites, in addition to 50 randomly selected mitochondrial HVR haplotypes. As we focus on neutrally evolving regions of the genome, we expect the number of segregating sites per RAD locus to follow a Poisson distribution of parameter λ equal to the mean number of segregating sites per locus, whose expected value $E(\lambda)$ converges towards the 'true' underlying constant substitution rate μ, multiplied by the total tree length for each locus. Thus, for a fixed tree length, λ becomes an estimator of μ. However, under the EBSP model, the observed number of segregating sites is taken as an estimator of λ, and consequently of μ. Therefore, we expect the inferred value of μ for each locus class to be a posterior probability of 'true' μ, conditional on the mean number of segregating sites observed for that class[19]. Thus, we fitted a log-linear model to the inferred substitution rates ($\mu_3=0.0159$, $\mu_4=0.0218$, $\mu_5=0.0275$, $\mu_6=0.0389$. Fitted model: intercept $i=-5.02$, slope $s=0.292$, $R^2=0.997$). A Poisson model of parameter λ equal to the mean observed number of segregating sites was a good fit for the empirical distribution of the number of segregating sites per locus ($\lambda=1.47$, chi-squared test of goodness-of-fit *P* value = 0.232). Thus, we extracted μ as $e^{(si+i)}\sim1.02\times10^{-2}$ substitutions per site per million years, or 1.08×10^{-7} substitutions per site per generation. EBSP reconstruction shows only one bottleneck, and places it around 40 ka, between the two stairway-inferred bottlenecks (Supplementary Fig. 5)—an expected behaviour according to our simulation tests (see below).

Pairwise Sequentially Markovian Coalescent (PSMC'), another model-flexible method, allows for accurate reconstruction of deeper-time demographic events without prior specification, although it lacks power for more recent time periods[72,73]. Since recombination events are treated as a Markovian process along the sequence, we can increase the likelihood of the reconstruction by concatenating several genomes, thus increasing the independent sampling of the Time to Most Recent Common Ancestor (TMRCA). For each species, the analysis was run on all three samples simultaneously, with 200 bootstrap replicates. Substitution rate and generation time were defined as above. The results (Supplementary Fig. 6) are very similar to the EBSP analysis (Supplementary Fig. 5). However, the resolution of the PSMC' analysis is low for the recent past, and the latest five time bins exhibit

© 2018 Macmillan Publishers Limited, part of Springer Nature. All rights reserved.

considerable instability (Supplementary Fig. 6A). The exact timing of the LGM bottleneck is not precisely retrieved for the king penguin: the two-step expansion since the mid-Pleistocene (Fig. 2) appears as one single bottleneck—also an expected behaviour according to our simulation tests (see below).

We simulated genetic data under the stairway-plot-inferred demographic model for the king penguin, and analysed it using all three algorithms. Data were generated in scrm[74] under a sequential Markovian coalescent model, matching the characteristics of our empirical data, and were converted either to a DAFS, or to sequence data in seq-gen[75]. We replicated the full simulation 200 times for confidence interval estimation. Whereas the stairway plot retrieves the principal events in the simulation (Supplementary Fig. 7A), both EBSP and PSMC' lack the resolution at this timescale. EBSP globally matches the expected demographic history (Supplementary Fig. 7B), with the simulated demography nearly entirely included in the EBSP 95% confidence interval, but the double bottleneck in our simulated data is smoothed out in the reconstruction. This is not surprising, however, given that EBSP includes only a subset of 50 short loci whereas the stairway plot is using the information from every genotyped SNP. PSMC' reconstruction, however, exhibits a more unexpected behaviour. Assuming equal substitution and recombination rates, none of the simulated bottlenecks is retrieved, but one single bottleneck is inferred instead around 40 ka, while a large population size peak is inferred in the early Holocene (Supplementary Fig. 7C). Decreasing the recombination rate to 1/16th of the substitution rate, both bottlenecks are retrieved, but the additional population depression remains around 40 ka, as well as a sharp population peak after the most ancient bottleneck (Supplementary Fig. 7D). However, the very recent events on which we focus may be at the limit of the PSMC' method[72].

Environmental data. We used sea surface temperature (SST) to model the APF position and its distance from each sub-Antarctic island (see the Assessment of the APF location section) and sea-ice concentration (SIC) to take into account winter sea ice around each island (see the Assessment of winter sea-ice concentration section). SST and SIC data were extracted from the latest generation of atmosphere–ocean general circulation models (from the Intergovernmental Panel on Climate Change CMIP5[76,77]) and we used a multi-model ensemble approach as follows. We selected 15 atmosphere–ocean general circulation models on the basis of the range of available outputs and their coverage of the Southern Ocean (Supplementary Table 3). Outputs were obtained from the Earth System Grid Federation (pcmdi9.llnl.gov/). We calculated the ensemble mean and standard deviation of SST and SIC using the CDO toolset (CDO 2015, http://www.mpimet.mpg.de/cdo). Reconstructions were performed under LGM, mid-Holocene and historical conditions, and projections for the twenty-first century, under three RCPs (RCP2.6, RCP4.5 and RCP8.5).

Biophysical ecological niche modelling. The ecological niche model for the king penguin was based on three major biophysical constraints: presence of insular (that is, predator-free) and ice-free land[24]; foraging distance of the prey stock at the APF[30] (see the Assessment of the APF location section); and low sea-ice concentration during winter for over-winter chick-rearing[24] (see the Assessment of winter sea-ice concentration section). Taken together, these three binary requirements define a grid to score locations in the Southern Ocean as suitable or unsuitable for the king penguin.

Assessment of the APF location. To assess the APF location, we followed a protocol similar to one that was published previously[20]. The 5 °C SST isotherm in February was used as a diagnostic of the position of the APF[78] where the king penguin is known to forage during the early chick-rearing stage, when constraints on foraging behaviour are especially strong[20]. Cell-by-cell (1°x1°) linear correlation of modelled and satellite-derived SST (National Oceanic and Atmospheric Administration (NOAA) Optimal Interpolation v2 SST data set[79]) from December 1981 to December 2005 was assessed and R^2, slope and intercept were plotted to assess the spatial distribution of the model departure from the observed values. As modelled SST was generally higher than observed SST in the APF zone over the historical period, we followed ref. [20], linearly correcting modelled values to match observed data (Supplementary Table 4). To maximize the fit, we defined four oceanic sectors: South Atlantic Ocean (45° W–18° E), south Indian Ocean (18° E–80° E), Macquarie (135° E–180° E) and the Falkland region (75° W–45° W), ranging in latitude from 45° S to 55° S, or 60° S in the Falkland region to account for the higher latitude of the APF around Cape Horn. The distance between each island and the 5 °C SST isotherm was calculated using GDAL (www.gdal.org) and the OGR Python library. Our foraging range predictions for the historical period closely matched both observed historical SST, and published foraging distances at most locations: ~380 km on Crozet (observed: 300–500 km), ~320 km on Marion (observed: 300 km three decades ago[80]), ~20 km in Kerguelen (observed: 270 km along the APF[81,82]—foraging trips extend latitudinally within nearby the productivity zone), ~310 km on Heard (observed: 370 km a decade ago[83]) and ~300 km in South Georgia (observed: 300–600 km over the whole breeding season[82]). The predicted distance for Macquarie Island (~240 km) is lower than the observed summer range (300–500 km; ref. [84]); however, recorded foraging trajectories meet the APF in the higher-productivity areas on the break of the Campbell Plateau rather than southward along the shortest route. Predicted and observed ranges differ most in the Falklands (predicted: ~640 km and observed: 300–500 km); however, the small Falkland population (and possibly the population in Tierra del Fuego) frequently forages on the Patagonian shelf break, and not directly on the APF[42]. This behaviour makes the local response to APF displacement uncertain, as other productivity areas may remain available. However the Patagonian Shelf, being under increasing pressure from overfishing and climate change[85], may be unable to sustain a large king penguin population[26].

Assessment of winter sea-ice concentration. Winter SIC limits the king penguin's southward expansion, as its over-winter breeding cycle makes year-round open-water conditions a requisite[24]. We consider the sea-ice extent (SIE) at its maximum (August and September), taking the 15% SIC isoline as representative of the ice edge[86]. Compared to satellite-derived measures from the NOAA Optimal Interpolation data set, reconstructed winter SIC tends to be denser than observed (mean SIC above 15% concentration over the 1981–2005 period: reconstructed $85 \pm 20\%$; observed $61 \pm 22\%$, t-test P value $< 2.2\times10^{-16}$), but less extended (reconstructed September SIE with SIC > 15% on the 1981–2005 period occupies 90% of observed SIC > 15% extent), although correlation is strong on a per-cell basis (mean $R^2 = 0.67 \pm 0.27$). Winter SIE is projected to decrease in all forcing scenarios. While SIC should still be high in the South Sandwich Islands during the last two decades of the century (RCP2.6: 0.26 ± 0.058, RCP4.5: 0.22 ± 0.044, RCP8.5: 0.045 ± 0.040), Bouvet Island is projected to become ice-free all year round by 2080 under all forcing scenarios (RCP2.6: 0.058 ± 0.037, RCP4.5: 0.028 ± 0.024, RCP8.5: 0.00041 ± 0.00053). SIC projections may not be quite as reliable as SST projections, but tend to underestimate true SIC[86–88]: in that case, king penguin range reduction may be even more drastic than we forecast here, as Bouvet may not be ice-free before the end of the century.

Uncertainty assessment of the modelling approach. To assess uncertainties in our modelling approach, we followed a previous study[89] by calculating the density distribution of projected foraging distance based on each climate model separately for each island: for the current period (2006–2015), for the middle of the century (2041–2050), and for the end of the century (2091–2100) (Supplementary Fig. 8). We also calculated the percentage of models forecasting local king penguin population collapse (February foraging distance > 700 km), as proposed previously[90]. The latitude of the APF, and therefore the duration of the king penguin's foraging trips, is subject to a high interannual variability, in particular under the influence of the cyclical El Niño/Southern Oscillation and Southern Annular Mode, with year-to-year latitudinal fluctuations of up to 200 km. Therefore, we considered that a location had reached its critical foraging distance when the foraging distance was greater than 700 km for at least 20% of a consecutive decade. Variability between models remains relatively high, as has already been observed in previous studies[89,91]. However, the strong consensus both in the increasing foraging distance trend, and in the actual prediction for local extinction, stresses both the very likely nature of the threats to the Southern Ocean ecosystems under the RCP8.5 scenario, and, yet, the possibility of avoiding the most destructive effects of these threats if immediate action allows us to bring greenhouse gas emissions closer to the RCP2.6 forcing scenario.

Data availability. Genetic data that support the findings of this study have been released and are publicly available in GenBank Short Reads Archive database (RADseq data, BioProject PRJNA308448, WGS data, BioProject PRJNA419826). Climatic data were downloaded from https://esgf-node.llnl.gov/projects/esgf-llnl/.

Further details about data and methods are provided in Supplementary Information.

References

52. Li, C. et al. Two Antarctic penguin genomes reveal insights into their evolutionary history and molecular changes related to the Antarctic environment. *Gigascience* **3**, 27 (2014).
53. Zhou, Q. et al. Complex evolutionary trajectories of sex chromosomes across bird taxa. *Science* **346**, 1246338 (2014).
54. DePristo, M. A. et al. A framework for variation discovery and genotyping using next-generation DNA sequencing data. *Nat. Genet.* **43**, 491–498 (2011).
55. Korneliussen, T. S., Albrechtsen, A. & Nielsen, R. ANGSD: Analysis of Next Generation Sequencing Data. *BMC Bioinformatics* **15**, 356 (2014).
56. Guindon, S. et al. New algorithms and methods to estimate maximum-likelihood phylogenies: assessing the performance of PhyML 3.0. *Syst. Biol.* **59**, 307–321 (2010).
57. Yang, Z. PAML 4: phylogenetic analysis by maximum likelihood. *Mol. Biol. Evol.* **24**, 1586–1591 (2007).
58. Hanson-Smith, V., Kolaczkowski, B. & Thornton, J. W. Robustness of ancestral sequence reconstruction to phylogenetic uncertainty. *Molecular Biol. Evol.* **27**, 1988–1999 (2010).
59. Langmead, B. & Salzberg, S. L. Fast gapped-read alignment with Bowtie 2. *Nat. Methods* **9**, 357–359 (2012).

© 2018 Macmillan Publishers Limited, part of Springer Nature. All rights reserved.

60. Excoffier, L., Laval, G. & Schneider, S. Arlequin (version 3.0): an integrated software package for population genetics data analysis. *Evol. Bioinform. Online* **1**, 47–50 (2005).
61. Reich, D., Thangaraj, K., Patterson, N., Price, A. L. & Singh, L. Reconstructing Indian population history. *Nature* **461**, 489–494 (2009).
62. Romiguier, J. et al. Comparative population genomics in animals uncovers the determinants of genetic diversity. *Nature* **515**, 261–263 (2014).
63. Fumagalli, M., Vieira, F. G., Linderoth, T. & Nielsen, R. ngsTools: methods for population genetics analyses from next-generation sequencing data. *Bioinformatics* **30**, 1486–1487 (2014).
64. Jombart, T. adegenet: a R package for the multivariate analysis of genetic markers. *Bioinformatics* **24**, 1403–1405 (2008).
65. Skotte, L., Korneliussen, T. S. SpringerAmpamp; Albrechtsen, A. Estimating individual admixture proportions from next generation sequencing data. *Genetics* **195**, 693–702 (2013).
66. Raj, A., Stephens, M. & Pritchard, J. K. fastSTRUCTURE: variational inference of population structure in large SNP data sets. *Genetics* **197**, 573–589 (2014).
67. Purcell, S. et al. PLINK: a tool set for whole-genome association and population-based linkage analyses. *Am. J. Hum. Genet.* **81**, 559–575 (2007).
68. Huson, D. H. & Bryant, D. Application of phylogenetic networks in evolutionary studies. *Mol. Biol. Evol.* **23**, 254–267 (2006).
69. Gutenkunst, R. N., Hernandez, R. D., Williamson, S. H. & Bustamante, C. D. Inferring the joint demographic history of multiple populations from multidimensional SNP frequency data. *PLoS Genet.* **5**, e1000695 (2009).
70. Saether, B. E. et al. Generation time and temporal scaling of bird population dynamics. *Nature* **436**, 99–102 (2005).
71. Millar, C. D. et al. Mutation and evolutionary rates in Adélie penguins from the Antarctic. *PLoS Genet.* **4**, e1000209 (2008).
72. Li, H. & Durbin, R. Inference of human population history from individual whole-genome sequences. *Nature* **475**, 493–496 (2011).
73. Schiffels, S. & Durbin, R. Inferring human population size and separation history from multiple genome sequences. *Nat. Genet.* **46**, 919–927 (2014).
74. Staab, P. R., Zhu, S., Metzler, D. & Lunter, G. scrm: efficiently simulating long sequences using the approximated coalescent with recombination. *Bioinformatics* **31**, 1680–1682 (2015).
75. Rambaut, A. & Grass, N. C. Seq-Gen: an application for the Monte Carlo simulation of DNA sequence evolution along phylogenetic trees. *Comput. Appl. Biosci.* **13**, 235–238 (1997).
76. Taylor, K. E., Stouffer, R. J. & Meehl, G. A. An overview of CMIP5 and the experiment design. *Bull. Am. Met. Soc.* **93**, 485–498 (2012).
77. Meijers, A. J. S. The Southern Ocean in the Coupled Model Intercomparison Project phase 5. *Phil. Trans. R. Soc. A* **372**, 20130296 (2014).
78. Moore, J. K., Abbott, M. R. & Richman, J. G. Location and dynamics of the Antarctic Polar Front from satellite sea surface temperature data. *J. Geophys. Res.* **104**, 3059–3073 (1999).
79. Reynolds, R. W., Rayner, N. A., Smith, T. M., Stokes, D. C. & Wang, W. An improved in situ and satellite SST analysis for climate. *J. Clim.* **15**, 1609–1625 (2002).
80. Adams, N. J. & Klages, N. T. Seasonal variation in the diet of the king penguin (*Aptenodytes patagonicus*) at sub Antarctic Marion Island. *J. Zool.* **212**, 303–324 (1987).
81. Koudil, M., Charrassin, J.-B., Le Maho, Y. & Bost, C.-A. Seabirds as monitors of upper-ocean thermal structure. King penguins at the Antarctic polar front, east of Kerguelen sector. *Comptes Rendus Acad. Sci.* **323**, 377–384 (2000).
82. Pütz, K. Spatial and temporal variability in the foraging areas of breeding king penguins. *Condor* **104**, 528–538 (2002).
83. Moore, G. J., Robertson, G. & Wienecke, B. Food requirements of breeding king penguins at Heard Island and potential overlap with commercial fisheries. *Polar Biol.* **20**, 293–302 (1998).
84. Wienecke, B. & Robertson, G. Foraging areas of king penguins from Macquarie Island in relation to a marine protected area. *Environ. Manag.* **29**, 662–672 (2002).
85. Halpern, B. S. et al. A global map of human impact on marine ecosystems. *Science* **319**, 948–952 (2008).
86. Turner, J., Bracegirdle, T. J., Phillips, T., Marshall, G. J. & Hosking, J. S. An initial assessment of Antarctic sea ice extent in the CMIP5 models. *J. Clim.* **26**, 1473–1484 (2013).
87. Xu, S. et al. Simulation of sea ice in FGOALS-g2: Climatology and late 20th century changes. *Adv. Atmos. Sci.* **30**, 658–673 (2013).
88. Shu, Q., Song, Z. & Qiao, F. Assessment of sea ice simulations in the CMIP5 models. *Cryosphere* **9**, 399–409 (2015).
89. Goberville, E., Beaugrand, G., Hautekèete, N. C., Piquot, Y. & Luczak, C. Uncertainties in the projection of species distributions related to general circulation models. *Ecol. Evol.* **5**, 1100–1116 (2015).
90. Raybaud, V. et al. Decline in kelp in west Europe and climate. *PloS One* **8**, e66044 (2013).
91. Cabré, A., Marinov, I., Bernardello, R. & Bianchi, D. Oxygen minimum zones in the tropical Pacific across CMIP5 models: mean state differences and climate change trends. *Biogeosciences* **12**, 5429–5454 (2015).

© 2018 Macmillan Publishers Limited, part of Springer Nature. All rights reserved.